EXPERIMENTAL AND NUMERICAL DETERMINATION OF THE PARAMETERS OF THE GURSON MODEL FOR DUCTILE FRACTURE

Vladislav Laš, Luboš Řehounek, Daniel Vavřík

Abstract

The paper presents results of numerical fit of axisymmetric FE model utilizing the modified Gurson model into experimental measurements of tensile strain and contraction evolutions of notched bars. This model combines plasticity and damage by introducing porosity of a material in order to predict final fracture. Although some of the parameters of the model can be determined by microscopic investigation of a specimen, the majority of the parameters need to be determined by fitting numerically obtained results into experimental ones. In this paper, it is shown that such a fit is achievable. However, the uniqueness of the obtained parameters is questionable.

Introduction

It has been observed that ductile fracture in metals can involve the generation of considerable porosity caused by nucleation, growth and coalescence of microvoids. This process takes place on micro-level and can not be described by traditional constitutive laws such as von Mises theory. Hence, A. L. Gurson introduced a model for ductile fracture [1] which includes the influence of hydrostatic stress on the evolution of plasticity condition. Coalescence of microvoids was incorporated later by A. Needleman and V. Tvergaard [2, 3]. The determination of the parameters describing the model need to be determined by fitting numerical results into experiments. Several procedures are mentioned in [3, 4]. The great advantage of this model is that the parameters have their physical interpretation and once they are obtained they can be transferred between different specimen regardless the geometry.

The purpose of this paper is to demonstrate a new possibility of obtaining the dominant parameters. It is based on measuring axial and radial deformations in several locations in the notch of a notched bar by video record processing. A detailed description of the experimental realization can be found in [8]. Further information related to the topic of this paper can be found in the works [5, 6].

Doc.Ing. Vladisla Laš, CSc., Ing. Luboš Řehounek, Západočeská univerzita v Plzni, Fakulta aplikovaných věd, katedra mechaniky, Univerzitní 22, 306 14 Plzeň, tel. 019/7491125, email: las@kme.zcu.cz, rehoun3@civ.zcu.cz
Ing. Daniel Vavřík, PhD., Ústav teoretické a aplikované mechaniky AV ČR, Prosecká 76, 190 00 Praha 9, tel. 02/86882121, email: vavrik@itam.cas.cz

Gurson Model

It assumes spherical voids surrounded by homogeneous, incompressible von Mises material (matrix). The model encompasses nucleation, growth and coalescence of voids and void volume fraction serves here as a damage parameter. Most of the parameters of the model need to be determined by fitting numerically obtained results into experiments. Ones these parameters are known they can be transferred between different specimen regardless their geometries.

Plasticity and local damage are combined by means of the yield function [1]:

$$\Phi = \frac{\sigma_e^2}{\sigma_M^2} + 2f \cosh\left(\frac{1}{2}\frac{\sigma_k^k}{\sigma_M}\right) - 1 + f^2 = 0$$

where f is void volume fraction, σ_M actual yield stress of the matrix material, σ_e von Mises equivalent stress and σ_k^k the trace of the Cauchy stress tensor.
For the description of the matrix material the linear-exponential law is frequently used:

$$\epsilon_M = \frac{\sigma_M}{E} \quad \text{for} \quad (\sigma_M > \sigma_y) \qquad \text{and} \qquad \epsilon_M = \frac{\sigma_M}{E}\left(\frac{\sigma_M}{\sigma_y}\right)^n \quad \text{for} \quad (\sigma_M > \sigma_y)$$

where n is hardening coefficient. Alternatively, true σ - true ϵ diagram can be used, instead.

The void evolution consists of two terms, namely the nucleation a growth rates. :

$$\dot{f} = \dot{f}_{nucl} + \dot{f}_{growth} \qquad \text{with initial condition} \quad f(t_o) = f_o$$

The nucleation part of $\dot{f}$ controlled by deformation can be expressed as:

$$\dot{f}_{nucl} = \frac{f_N}{s\sqrt{\pi}}\dot{\epsilon}_N^p \left[-\frac{1}{2}\left(\frac{\epsilon_M^p - \epsilon_N}{s}\right)^2\right]$$

where f_N is volume fraction of void nucleating particles, ϵ_N mean nucleation equivalent plastic strain, ϵ_M^p equivalent plastic strain of the matrix material and s standard deviation. For most metal alloys, voids nucleate from large inclusions and second phase particles by either particle fracture or interfacial decohesion.

The growth rate expressing the growth of already existing voids is assumed proportional to hydrostatic part of the stress tensor: $\dot{f}_{growth} = (1-f)\,\dot{\epsilon}_k^{kp}$
where $\dot{\epsilon}_k^{kp}$ is the trace of the plastic equivalent rate tensor.

Void volume fraction f follows the equations mentioned above until it reaches a critical value f_c. From this point, modified void volume fraction f^* is introduced (see [2]) and its evolution is accelerated in order to approximately describe the final stage before rupture during which coalescence of the individual voids takes place:

$$f^* = f \quad \text{for} \quad f \le f_c \qquad \text{and} \qquad f^* = f_c + \frac{f_u^* - f_c}{f_F - f_c}(f - f_c) \quad \text{for} \quad f > f_c$$

where f_F stands for final/fracture void volume fraction when the material looses its carrying capacity and f_u^* is defined as $f_u^* = f^*(f_F)$.

Microscopic quantities of the matrix material and macroscopic quantities describing “continuum” material are connected via the equality of plastic work: $(1-f)\,\epsilon_M^p \sigma_M = \epsilon^p \sigma$

Conclusion

The computed strain evolution curves are in satisfactory agreement with the curves obtained from the experiment. Nevertheless, the “try and see” process of finding meaningful values of so many parameters is far from a systematic approach. Therefore, there is a tendency to reduce the number of parameters.

In [7], for example, f_c becomes a field quantity and is a function of f_o, similarly as f_F. Further reduction of the number of parameters is achieved by introducing a simpler nucleation model characterized by one single parameter, only.

It is believed by the authors that the modifications suggested in [7] are worth following and will become the subject of the next research.

The paper was elaborated as a part of the Research project MSM 235200003 and the Grant GA ČR No 106/99/1467

References

[1] Gurson, A.L.: Continuum Theory of Ductile Rupture by Void Nucleation and Growth, J. Eng. Mat. Tech., Paper No. 76-Mat-CC, 1977

[2] Needleman, A., Tvergaard, V.: An Analysis of Ductile Rupture in Notched Bars, J. Mech. Phys. Solids Vol. 32, No. 6, Pergamon Press, 1984

[3] Tvergaard, V.: Material Failure by Void Growth to Coalescence, Academic Press, Inc., Denmark, 1990

[4] Brocks, W., Klingbeil, D., Kűnecke, G., Sun, D.Z.: Application of the Gurson model to ductile tearing resistance, American society for Testing and Materials, Philadelphia, 1995

[5] Laš, V., Řehounek, L.: Use of ductile damage models in the system MARC, Proceedings of MSC Software Users Meeting, Brno, 2000

[6] Laš, V., Řehounek, L.: Sensitivity Analysis of the Modified Gurson Model, Proceedings of Computational Mechanics 2000, Nečtiny, 2000

[7] Zhang, Z.L.: A Complete Gurson Model Approach for ductile Fracture, Eng. Fracture Mech. No. 67, Pregamon Press, 2000

[8] Vavřík, D.: Optical determination of constitutive equations parameters of nonlinear materials, Proceedings of EAN 2001, Tábor, 2001

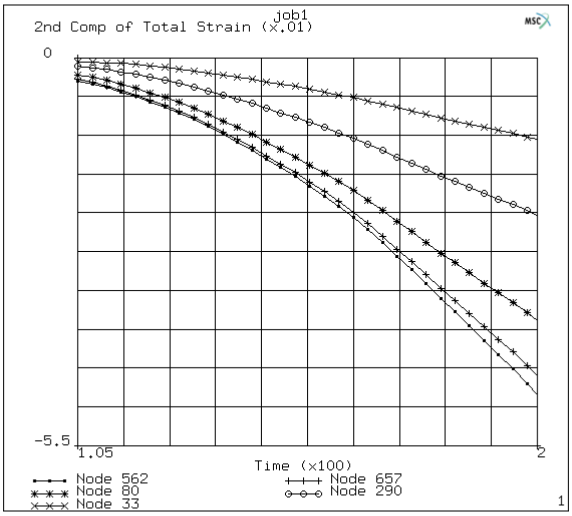

Fig.5 Model with damage behavior included

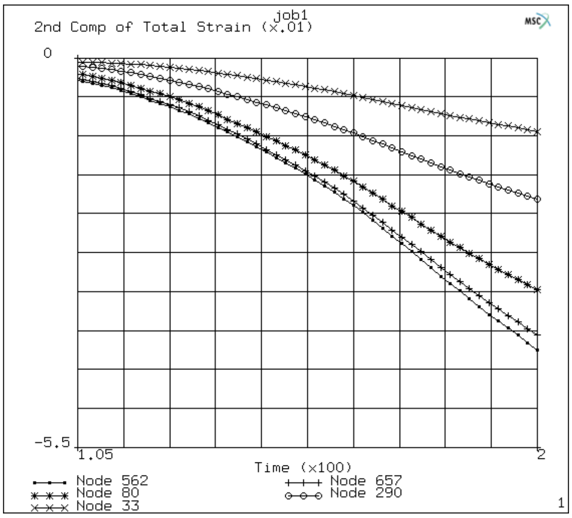

Fig.6 Model without damage

Fig.5 (referring to the model with the values from tab.1) and fig.6 (referring to the model with plasticity only, i.e. without damage) show time history of ε_{22} in the measuring nodes on the surface of the notch. It can be seen that damage behavior has some influence on both the shape and maximum values of the displayed curves.

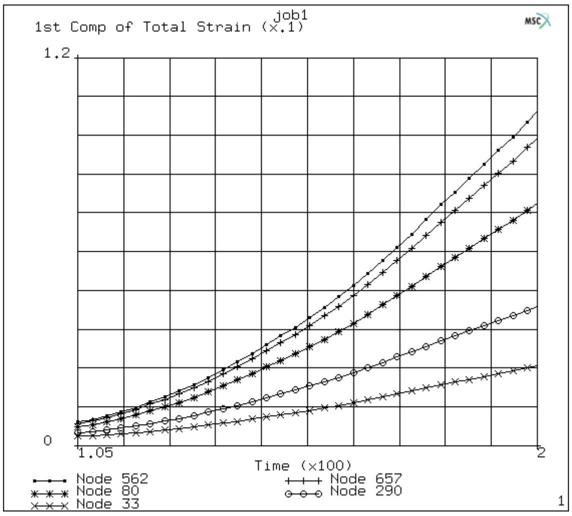

Fig.7 Model with damage behavior included

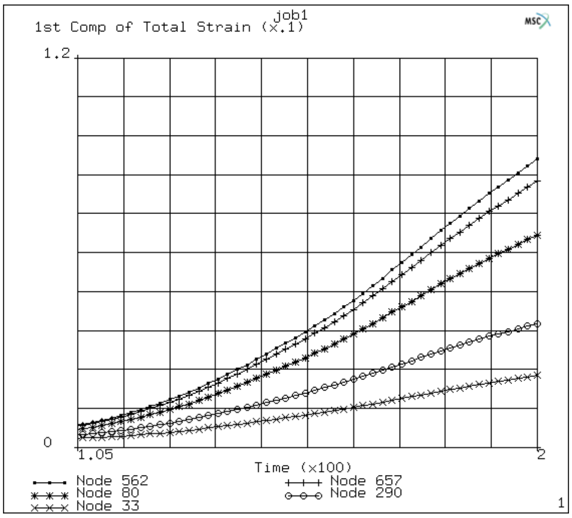

Fig.8 Model without damage

Fig.6 and fig.7 show time history of ε_{11} at the measuring nodes on the surface of the notch. Again, one can see that damage behavior has some influence on the shape and maximum values of the displayed curves.

It is probably not necessary to point out that the curves in fig.2 and fig.3 should be compared with the curves in fig.5 and fig.7, respectively – i.e. not with the curves in fig.2 and fig.3 which were included for illustrative purpose only. A detailed comparison of the influence of individual parameters will be presented elsewhere. Let us just state that f_O has a dominant role over the whole time history of tensile tests while f_C and f_C control more or less only the time of rupture.

The presented results should be viewed as a starting point for further research, both experimental and numerical, in other specific areas of mechanics – namely, nonlinear fracture mechanics of materials with ductile fracture.

Numerical Determination of the Gurson Model Parameters

As already mentioned, most of the parameters of the material model can only be determined by comparison between numerical and experimental results. The problem is, however, that during the experiments fracture appeared at relatively small strains (about 1/8 of the strains referred in literature). Hence, the space for numerical fitting was rather limited.

The mesh used for computations can be seen in fig.4. The working diagram of the aluminium alloy is in fig.5 (yield stress is 185 MPa) and the time history of the tensile force can be seen in fig.6. Tab.1 shown the values of material parameters which lead to a satisfactory fit into experimental results.

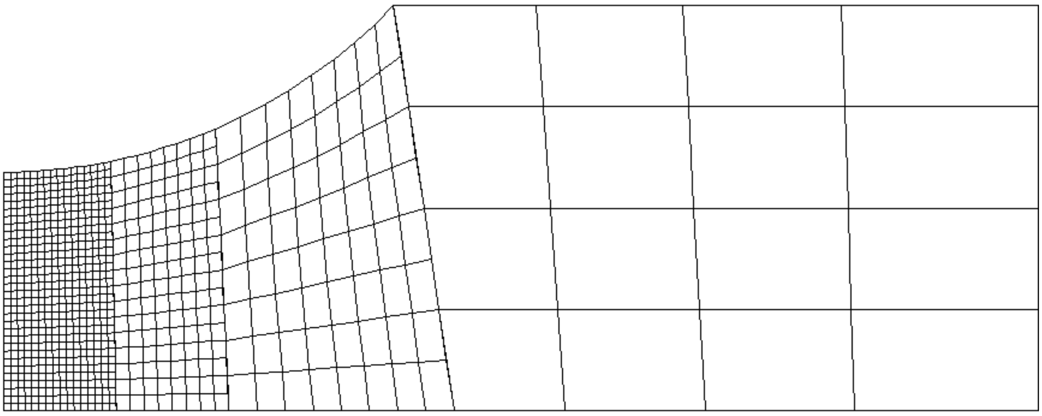

Fig.4 Finite element mesh used for most computations with measuring nodes

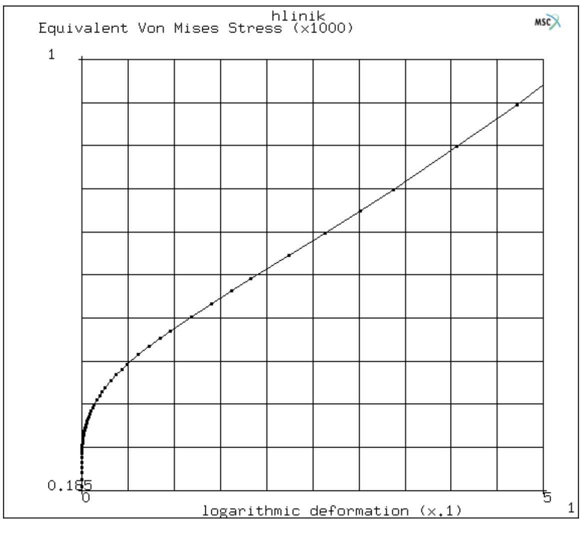

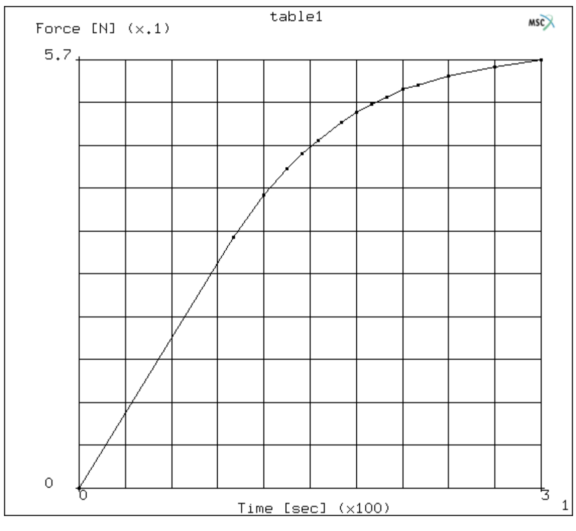

Fig.5 The working diagram of the material

Fig.6 The time history of the tensile force

f_O	f_C	f_F	ε_N	s_N	f_N
0.005	0.05	0.15	0.15	0.05	0.04

Tab.1 Values of the material parameters used for numerical simulation

Experimental Measurement

Details on experimental measurement can be found in [8] and is out of the scope of this paper. To sum up in one sentence, a tensile test was conducted on a notched specimen with measu-ring lines (see fig.1), which served for later evaluation of strains (see fig.2 and fig.3) by means of digital video camera record processing.

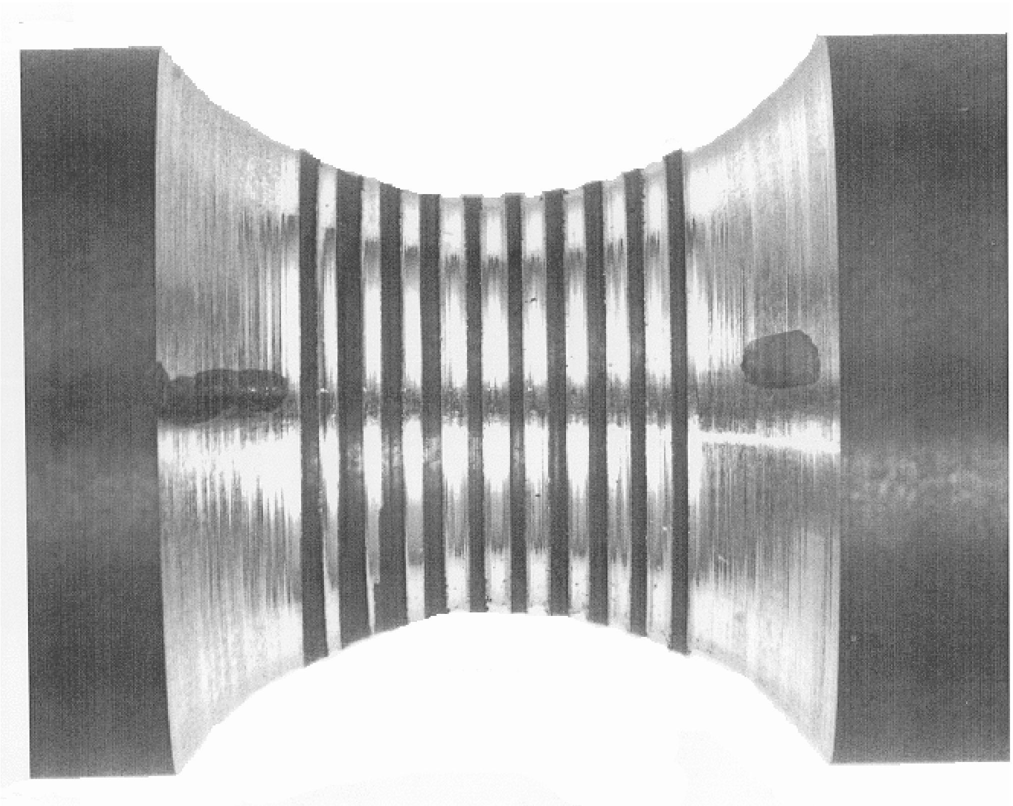

Fig.1 Detail of the notch of the test specimen with measuring lines

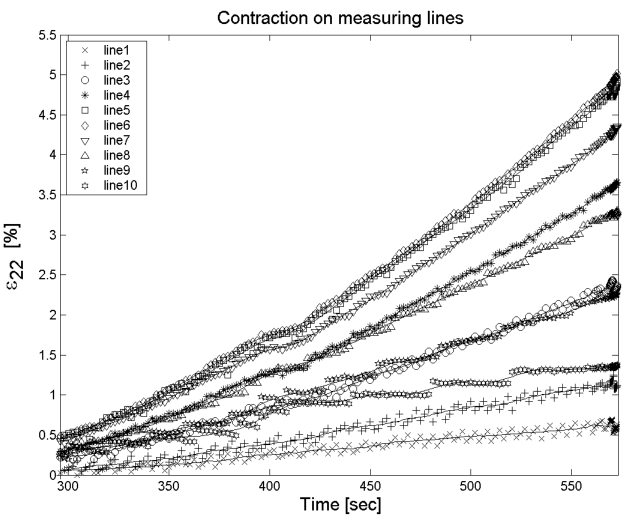

Fig.2 Radial contraction on measuring lines

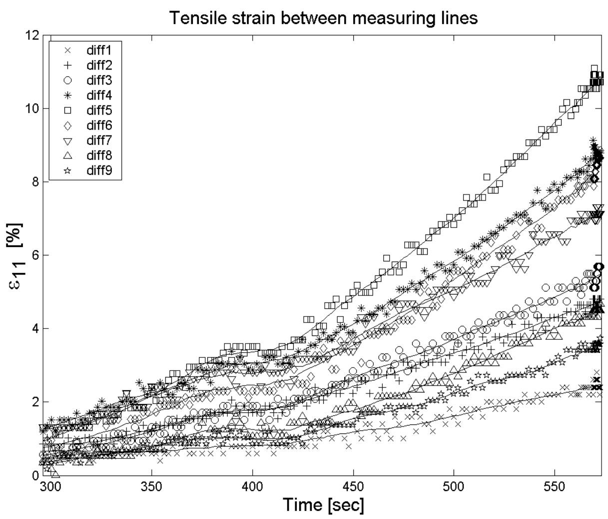

Fig.3 Tensile strain between measuring lines